Available online at www.sciencedirect.com
ScienceDirect
Trans. Nonferrous Met. Soc. China 33(2023) 2428−2438
Transactions of Nonferrous Metals Society of China
www.tnmsc.cn

Effects of transition metal elements and O on grain boundary energy and strength of Co by first-principles study

You-heng CHEN[1], Cui-ping WANG[1,2], Xiang HUANG[1], Chen YANG[1], Jia-jia HAN[1,2], Xing-jun LIU[1,3]

1. Fujian Provincial Key Laboratory of Materials Genome, College of Materials, Xiamen University, Xiamen 361005, China;
2. Xiamen Key Laboratory of High Performance Metals and Materials, Xiamen University, Xiamen 361005, China;
3. Institute of Materials Genome and Big Data, Harbin Institute of Technology, Shenzhen 518055, China

Received 4 February 2022; accepted 13 July 2022

Abstract: Considering the $\Sigma 5(210)[001]$ grain boundary of Co as a model, the influence of transition metals and their coupling with O on the grain boundary energy and strength was investigated by a first-principles-based study. Quantitative characterization was used to explain the transition metal segregation at the grain boundary, and the negative correlation between grain boundary energy and atomic radius was revealed. It has been found that the interaction between the solute and the host atoms at the grain boundary affects the grain boundary strength. Re, W, Os, Cr, Tc, Mo, Ir, Ta, Zr, Ru, Nb, V, Rh, Pt, Pd, and Ni can significantly strengthen the grain boundary, while other transition metals have a weakening effect on the grain boundary. In particular, Cr, Hf, Ta, W, Re, Os, Ir, and Pt can effectively alleviate the weakening of the grain boundary caused by O atoms.

Key words: transition metal elements; oxygen; Co-based superalloys; first-principles calculation; segregation; grain boundary energy; grain boundary strength

1 Introduction

The strengthening mechanisms in conventional Co-based superalloys made of Co solid solution and various carbides cannot provide sufficient strength and stability in high-temperature environments when compared with Ni-based superalloys [1]. With the first discovery of the γ' phase with ordered $L1_2$ microstructure embedded in the disordered γ phase in a Co−Al−W ternary system that is similar to the Ni-based superalloys, the novel Co-based alloys exhibit better high-temperature strength than conventional ones [2,3]. The solidus and liquidus temperatures of the novel Co-based alloys are 100−150 °C higher than those of the advanced Ni-based alloys [4], suggesting that they can surpass the limits of the temperature capability of Ni-based superalloys. To date, great efforts have been made to improve the oxidation resistance and mechanical properties of Co-based alloys [5−7]. Experiments indicate that the grain boundaries (GBs), in addition to the strengthening phases, play an important role in improving the mechanical properties as well as the oxidation resistance of superalloys [8,9]. BOCCHINI et al [10] pointed out that the coupling effect of the addition of B and Zr can improve the creep strength of the Co−Al−W ternary base alloy without forming borides at GBs. On the other hand, the presence of the GB will provide a rapid diffusive channel for oxygen [11]. In this way, oxides are easily formed at the GBs, thereby reducing the fracture toughness and fatigue resistance of the Co-based alloys. KLEIN et al [12]

Corresponding author: Xing-jun LIU, Tel: +86-592-2180606, Fax: +86-592-2187966, E-mail: xjliu@hit.edu.cn;
Jia-jia HAN, E-mail: jiajiahan@xmu.edu.cn
DOI: 10.1016/S1003-6326(23)66270-3

pointed out that the Ni in the Co−Al−W−B superalloy lowers the oxidation resistance, while Si enhances the formation of the Al_2O_3 protective layer, which improves the oxidation resistance of alloys. The complex behaviors of the elements at the GB found in these experiments indicate that a comprehensive understanding of the alloying elements as well as their interactions with oxygen at the GB is essential to effectively optimize the high-temperature mechanical properties of the alloy.

Nevertheless, the atomic structure and composition of the GBs are difficult to be determined by experimental measurements, and the physical nature of the observed phenomenon cannot be readily learned through experiments [13]. In this scenario, the theoretical calculation based on the density functional theory (DFT) is an alternative approach that can provide relevant information about the atomic and electronic structures, thermodynamic stability, and mechanical properties of the GBs. GB properties of Ni-based superalloys have been widely studied by theoretical calculations. These studies mainly focused on the effect of alloying elements and impurities on GB segregation and strength. For example, RAZUMOVSKIY et al [14] carried out a systematic study of the effects of transition metals as well as some nonmetallic elements on the GB cohesion of Ni-based alloys. They found that Zr, Hf, Nb, Ta, and B tended to move towards GB to improve the GB strength. In contrast, theoretical studies that focused on the GB properties of Co-based superalloys are yet limited [15]. The possible weakening of the GB caused by the segregation of O atoms at the GB is unclear. More importantly, the coupling effect of alloying elements and O atoms at the GB of Co-based superalloys has not been systematically investigated to the best of our knowledge.

In this work, a DFT-based first-principles method was applied to investigating the behavior of various transition metals (TMs) elements at the GB of face-centered cubic Co alloys. The construction of the GB models is based on the coincidence site lattice (CSL) theory. The symmetrical tilted $\Sigma5(210)[001]$ GB was employed to represent a general high-angle GB [16,17]. First, we explored the segregation tendency of different TM atoms at the GB. Then, the GB energy and strengthening potency energy were calculated, which helped evaluate the stability and strength of the GB, respectively. Then, we investigated the segregation behavior of O atoms at the GB doped with TM, aiming at revealing the effect of TM on the oxidation of GB from the perspective of GB energy and strengthening potency energy.

2 Grain boundary models and computation details

2.1 Construction of computational supercells

In the present work, $\Sigma5(210)[001]$ GB is selected based on the CSL approach. In CSL construction, it is assumed that two crystals on two sides of a GB interpenetrate, resulting in some shared lattice sites. These common sites form the CSL. The term Σ represents the reciprocal of the density of the coincident sites. The $\Sigma5(210)[001]$ GB is modeled by a 20-layer supercell with four atoms in each layer, as shown in Fig. 1. Substitutional and interstitial sites are denoted as index S and I, respectively. Due to the periodic boundary conditions, the model contains two GBs, and the two equivalent regions of the GB are represented by Region 1 and Region 2, respectively. The corresponding free surface (FS) model is constructed by removing the nine atomic layers above.

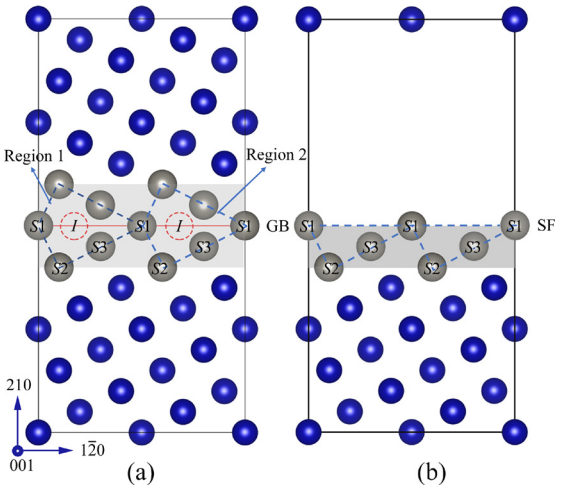

Fig. 1 Schematic illustration of Co $\Sigma5(210)[001]$ GB model based on CSL model (a) and corresponding FS model built by removing nine upper layers (b)

2.2 Segregation energy

To investigate the stability of different doping sites at GB, the GB segregation energy E_{seg}^{GB} is introduced as follows:

$$E_{seg}^{GB}=(E_{x,y}^{GB}-E_{0,0}^{GB})-(E_{x,y}^{Bulk}-E_{0,0}^{Bulk}) \quad (1)$$

where $E_{x,y}^{GB}$ and $E_{x,y}^{Bulk}$ represent the total energies of the GB and bulk models with doping elements x and y, respectively. In our case, x denotes the TM atom and y denotes the O atom. $E_{0,0}^{GB}$ and $E_{0,0}^{Bulk}$ represent the total energies of the pure GB and bulk models, respectively. The bulk model has the same number of atoms and shape as the GB model but contains no GBs. Analogously, the FS segregation energy E_{seg}^{FS} is calculated by

$$E_{seg}^{FS}=(E_{x,y}^{FS}-E_{0,0}^{FS})-(E_{x,y}^{Bulk}-E_{0,0}^{Bulk}) \quad (2)$$

In this definition, a negative value corresponds to a stable segregation site. For the better understanding of the segregation behavior, the McLean−Langmuir isotherm model [18] related to the segregation energies was used to evaluate the concentration of TMs at the GBs at finite temperatures:

$$\frac{c_k}{1-c_k}=\frac{c_0}{1-c_0}\exp[-E_{seg}^{GB}/(k_BT)] \quad (3)$$

where c_0 and c_k are the occupancies of the bulk and substitutional site of the TMs, respectively, T is the temperature, and k_B is the Boltzmann constant. At elevated temperatures, sites with negative E_{seg}^{GB} are likely to be occupied. The average concentration at GBs is described as $\langle c_k\rangle=1/N\sum_k c_k$, where N is the number of the substitutional sites at GBs. In this way, the effective segregation energy $\tilde{E}_{seg}^{GB}$ can be expressed as

$$\tilde{E}_{seg}^{GB}=k_BT\left[\ln(\frac{c_0}{1-c_0})-\ln(\frac{\langle c_k\rangle}{1-\langle c_k\rangle})\right] \quad (4)$$

Then, the effective solute concentration ($\tilde{c}$) is expressed as

$$\tilde{c}=\frac{c_0\exp[-\tilde{E}_{seg}^{GB}/(k_BT)]}{1-c_0\exp[-\tilde{E}_{seg}^{GB}/(k_BT)]} \quad (5)$$

Under the limit of dilute solution, the bulk occupancy c_0 is considered to be 1 at.% and the related partitioning coefficient (K) is expressed as

$$K=\tilde{c}/c_0 \quad (6)$$

2.3 GB energy

The GB energy $\gamma_{x,y}^{GB}$ is defined as the energy required to create a GB. In our models, the GB/FS energy without doping is defined by $\gamma_{0,0}^{GB}=(E_{0,0}^{GB}-E_{0,0}^{Bulk})/(2A)$, where A is the cross-section area of the supercell. The doped GB/FS model shown in Fig. 1 contains two interfaces: one without doping and the other with doping, and thus, the energy of the doped GB/FS is described as

$$\gamma_{x,y}^{GB}=(E_{x,y}^{GB}-E_{x,y}^{Bulk})/A-\gamma_{Pure}^{GB} \quad (7)$$

It is noted that Eqs. (1) and (7) are similar because the GB energy is directly related to the segregation behavior. That is, the driven force of segregation towards GB is equivalent to the reduction of GB energy.

2.4 Strengthening potency energy

The strength of GB can be evaluated by the Rice−Wang model [19]. We use the strengthening potency energy (η) [18] to characterize the strengthening effect of dopants, which is defined as

$$\eta=E_{seg}^{FS}-E_{seg}^{GB} \quad (8)$$

In this definition, a positive or a negative value of η indicates the strengthening or weakening effect, respectively. To better understand the strengthening effect of different TMs on GB, η is decomposed into mechanical (η_{mech}) and chemical (η_{chem}) contributions, which result from structural distortion around the TM atoms and electronic interactions between the TM atom and surrounding host Co atoms [18,20,21].

Figure 2 illustrates the details of the calculation. Figure 2(a) shows the relaxed GB/FS structure containing a TM atom. The value of η can be obtained by calculating the GB/FS segregation energies. Figure 2(b) shows the GB/FS model with the TM vacancies, which are generated by removing the TM atom from Fig. 2(a) but without further structural relaxation. The chemical component is calculated by

$$\eta_{chem}=\eta-\eta_{mech} \quad (9)$$

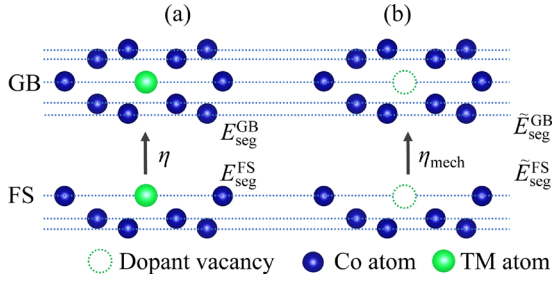

Fig. 2 Schematic illustration for calculation of strengthening potency energy (a) and its mechanical component (b)

2.5 Calculation details

All calculations were performed based on the density functional theory (DFT) using the projector augmented wave pseudopotential method [22], which was implemented in the Vienna ab-initio simulation package (VASP) [23]. The generalized gradient approximation (GGA) of Perdue−Burke−Ernzerhof (PBE) [24] was used for the exchange and correlation energy. The cut-off energy of the plane-wave basis was set to 350 eV to ensure convergence. The Brillouin zone (BZ) was sampled using a $3 \times 3 \times 2$ k-mesh in the Monkhorst−Pack scheme [25]. In the ionic relaxation calculations, the Methfessel−Paxton technique [26] was used for reciprocal integration with a smearing width of 0.15 eV. The convergence criteria for total energy and force were set to be 1×10^{-5} eV and 1×10^{-2} eV/Å, respectively. Spin polarization was considered due to the ferromagnetic nature of Co-based materials.

3 Results and discussion

3.1 Segregation behaviors of TMs

Figure 3 shows the segregation energy E_{seg}^{GB} of TMs at the $S1$, $S2$, and $S3$ sites of the GBs. When TMs occupy the $S1$ site, E_{seg}^{GB} is negative, while for the $S2$ and $S3$ sites, the sign of E_{seg}^{GB} depends on the element type. The results show that all TMs except Y and Zr prefer to occupy the $S1$ site, and the negative value ensures the thermodynamic stability of TMs during their segregation at the GBs. Since γ'-strengthened Co-based superalloys generally work in high-temperature environments, we evaluated the effective solute concentration of TMs at 800 K based on the McLean−Langmuir isotherm model, and the results are shown in Fig. 4. For each period, the partition coefficient for the elements from the early TM to the later TM shows an approximate U-shaped regular change. According to our calculations, Y has a strong segregation tendency at GBs and 800 K compared to other TMs. This result is in good agreement with the experimental observation [27], which confirms the full segregation of Y at GBs. Similarly, it was found experimentally that Zr is also strongly inclined to segregate at the GBs, which is completely consistent with the results of our calculation [10].

It is noteworthy that owing to the limited substitution sites at GBs, there is a competitive effect between the segregated atoms. When multiple segregations exist in the system, the segregation energy, in addition to the partition coefficient, should be considered to evaluate the degree of segregation reasonably. For example, the experimental results show that W has a strong segregation tendency at the GBs. However, when Zr is present, the segregation of W will be suppressed

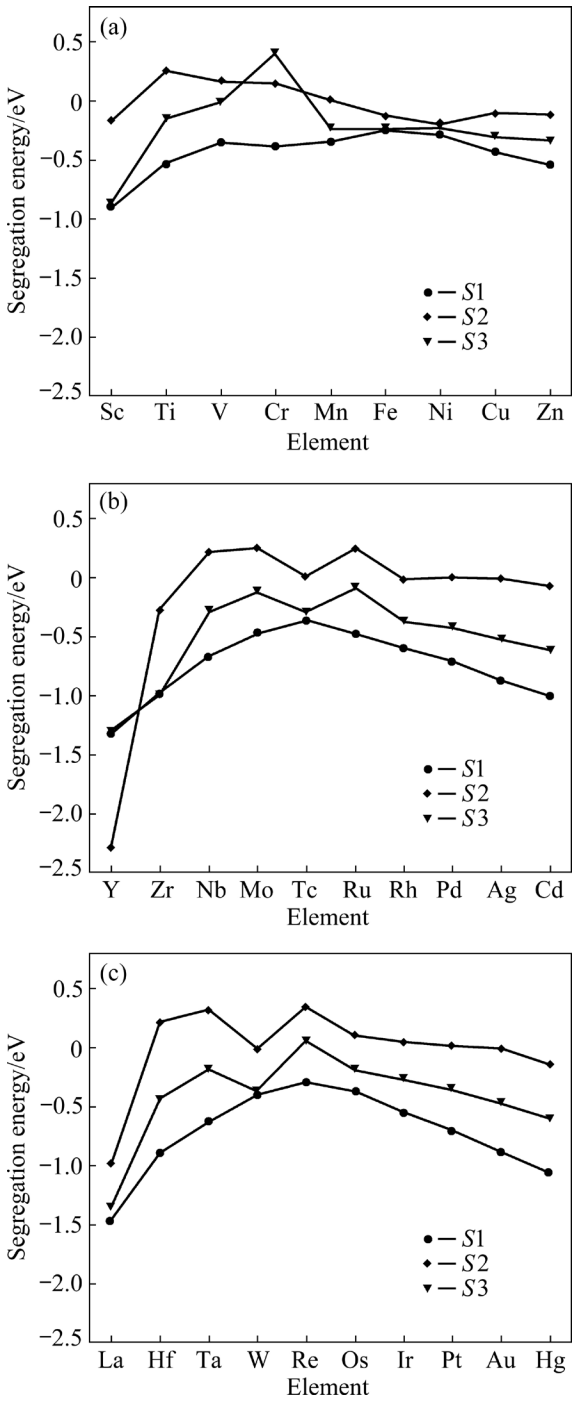

Fig. 3 Segregation energy of 3d (a), 4d (b) and 5d (c) TMs at substitutional sites of GBs (Negative values indicate stable substitutional sites for TMs)

largely [10]. According to the results in Fig. 4, W has negative E_{seg}^{GB} at *S*1 and *S*3 and positive E_{seg}^{GB} at *S*2, which indicates that W tends to segregate only at *S*1 and *S*3. Meanwhile, Zr also tends to segregate at *S*1 and *S*3, with a more negative E_{seg}^{GB}. Therefore, Zr, compared with W, has an advantage in thermodynamics in occupying the sites at GBs. This thermodynamically explains why the segregation behavior of Zr atoms is severely hindered in the presence of W atoms observed in experiments.

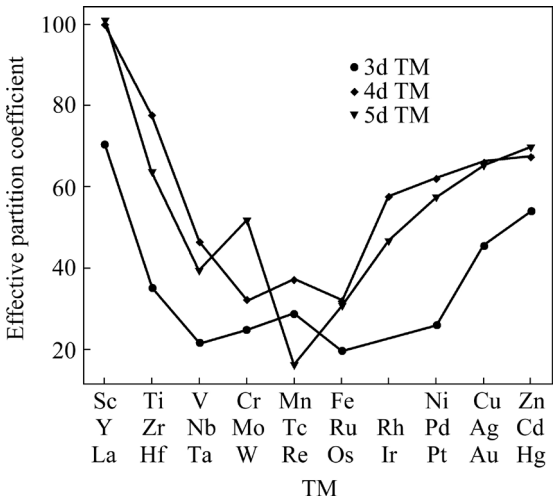

Fig. 4 Effective partition coefficients (*K*) at 800 K and bulk concentration of 1 at.%

3.2 Strengthening effects of TMs

Figure 5(a) shows the GB energy with each TM at the most stable site, where each period is presented by an independent line. As expected from the definition, the profile of the GB energy with dopants in each period is similar to that of the segregation energy of TM, namely, the GB energy is decreased due to segregation at GB. Figure 5(b) illustrates the relationship between GB energy and the atomic radius of TMs. It is found that there is a notable negative correlation between the atomic radius of the TMs and the GB energy. The larger the TM radius, the lower the GB energy, resulting in a stronger tendency to segregate in the GBs [7,17].

The calculated strengthening potency energy η of the GBs by TMs is shown in Fig. 6. We can see that the η of the segregated elements at the GBs also exhibits periodic characteristics like the GB energy. As per the definition, most of the segregated TMs have a strengthening effect on the GBs, which is most obvious in the TMs located in the middle of each period. On the contrary, both early and later

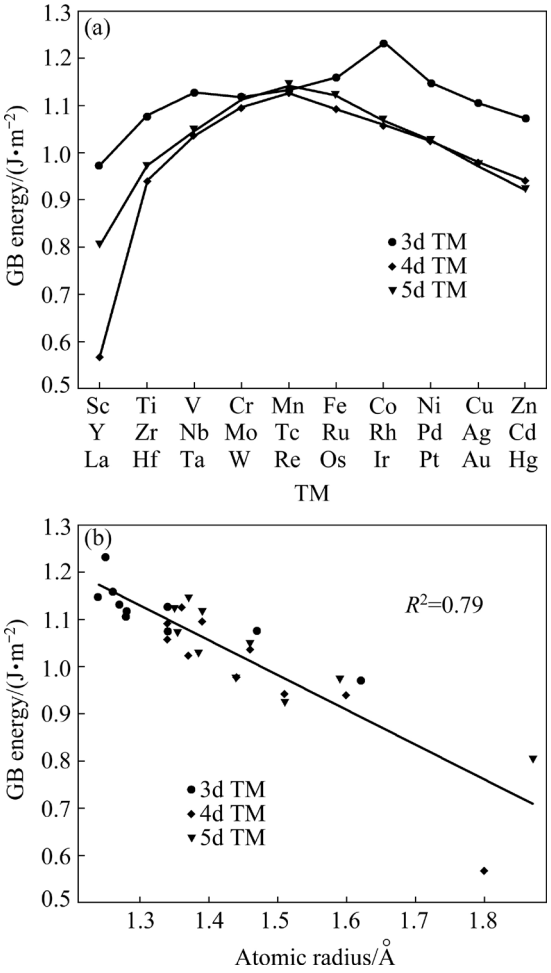

Fig. 5 Energy of GBs doped with TMs at their most stable substitutional sites (a), and relationship between GB energy and atomic radius of TMs (b)

TMs show a weakening effect. Generally, the strengthening or weakening effect is a result of two mechanisms: local distortion induced by segregation at the GBs; the charge redistribution between the impurity atoms and host atoms. Hence, we divided the strengthening potency energy into the mechanical and chemical components. For 3d elements, most of the mechanical components are negative and show little change except Sc. Thus, the total change tendency of η depends on the chemical components. On the contrary, for 4d elements, most of the mechanical components are positive. The weakening effects of Ag and Cd may be attributed chiefly to the negative chemical components. For 5d elements, the changing patterns of the total, mechanical and chemical components are similar, and the pronounced strengthening effects in the middle of the period are the result of the synergetic effect of the mechanical and chemical components.

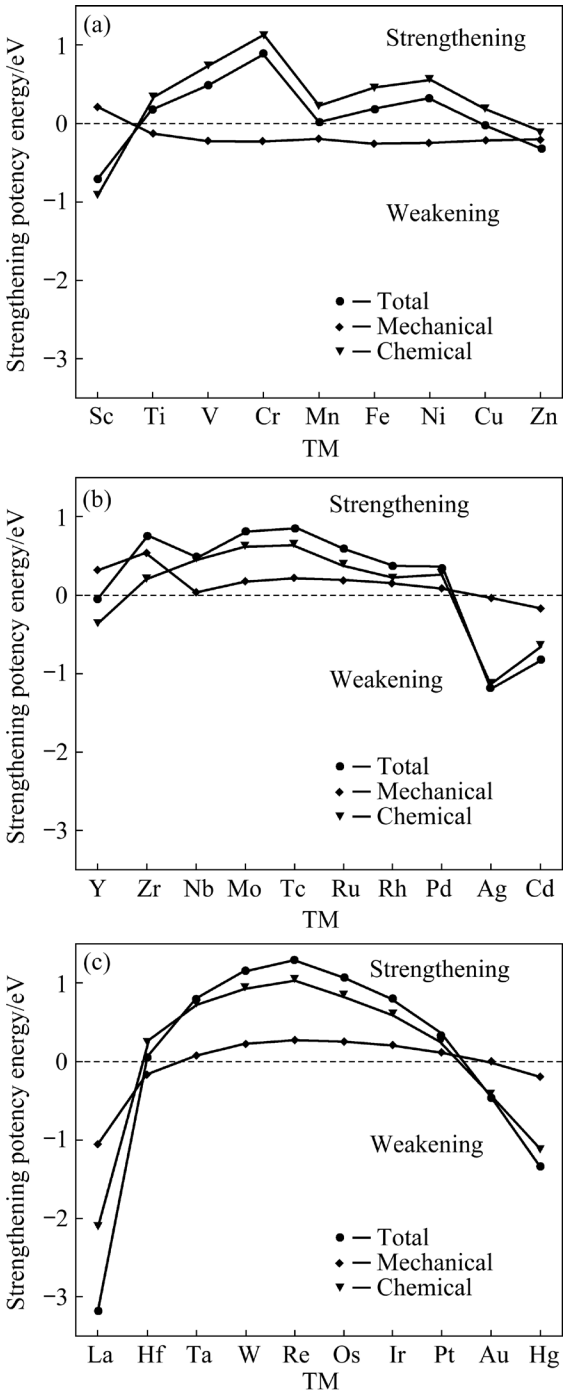

Fig. 6 Strengthening potency energy and its mechanical and chemical components of 3d (a), 4d (b) and 5d (c) TMs

To get a deeper understanding of the electronic interactions between TM atoms and host Co atoms, the charge density difference (CDD) ($\Delta\rho$) is introduced as follows:

$$\Delta\rho=\rho_{sc}-\rho_{atom} \tag{10}$$

where ρ_{sc} and ρ_{atom} are the self-consistent and non-self-consistent charge densities of the supercell, respectively. Four elements (Cu, Ni, Zn, and Ir) are selected to reveal the relationship between CDD and strengthening potency energy, where the magnitude of the chemical components is ranked as: $\eta^{Ir}_{chem} > \eta^{Ni}_{chem} > 0 > \eta^{Cu}_{chem} > \eta^{Zn}_{chem}$. Figure 7 shows the CDD at the GBs. The charge transfer between different TMs and neighboring Co atoms differs quantitatively. When the segregated atom is Cu or Zn (Figs. 7(a) and (c)), it is observed that the charge transfer between Cu or Zn and Co1−4 is depleted, indicating a weak interaction between the segregated atom and the matrix atom, thereby weakening the GBs. When Ni atoms occupy the *S*1 site of the GBs, the charge transfer between the Ni−Co atomic pairs is largely increased, and the strong interaction between the original Co−Co atom pairs is maintained, thereby strengthening the GBs. This phenomenon is more pronounced when Ir serves as the segregated atom, which is responsible for the largest GB strengthening effect in these four cases.

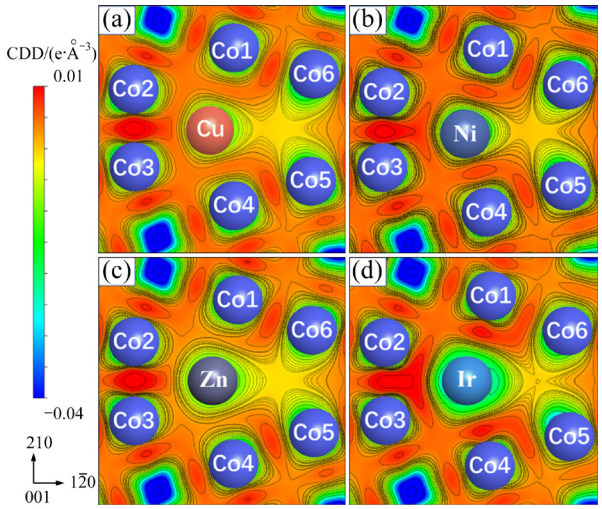

Fig. 7 CDD plots of (001) plane of GBs doped with Cu (a), Ni (b), Zn (c) and Ir (d)

Figure 8 shows the partial density of states (PDOS) of the GBs with the segregation of Cu, Ni, Zn and Ir atoms. Here, we focus on the d-orbital interaction between the segregation atom and the Co atom because of its dominant effect on the bonding strength. As can be seen, the segregation of Cu, Ni, and Ir atoms has large overlapping regions about the d-orbit with Co atoms, which is a sign of strong d-electron hybridization between the atoms at the GBs. From the notable PDOS of the anti-bonding orbit, the PDOS of Ir overlaps with

that of Co to a greater extent. This strong d-electron hybridization results in high GB strength. In contrast, the d-electron of the Zn atom is highly localized and hardly overlaps with the d-electron of Co atoms, which is responsible for the weakened GBs when Zn serves as a segregation atom.

3.3 TM-segregated GBs with O impurities

The segregation behavior of TMs at GBs, including their influence on GB energy and GB strength has been elucidated. Next, we will discuss the coupling effect of TM and O atoms on the properties of GBs. Previous studies have shown that the existence of nonmetallic impurities does not change the most stable sites of metallic dopants [20]. Therefore, we keep TMs in their original most stable state, and on this basis, consider the case of two inequivalent interstitial sites for the O atoms (see Fig. 9).

Figure 10 shows the segregation energy E_{seg}^{GB} of O atoms at different interstitial sites of GBs in the presence of various TMs. It is apparent that the existence of TMs drastically changes the segregation behavior of O atoms, by comparing the reference state shown by the horizontal dotted line. According to the definition, Ti, V, Cr, Mn, Fe, Zr,

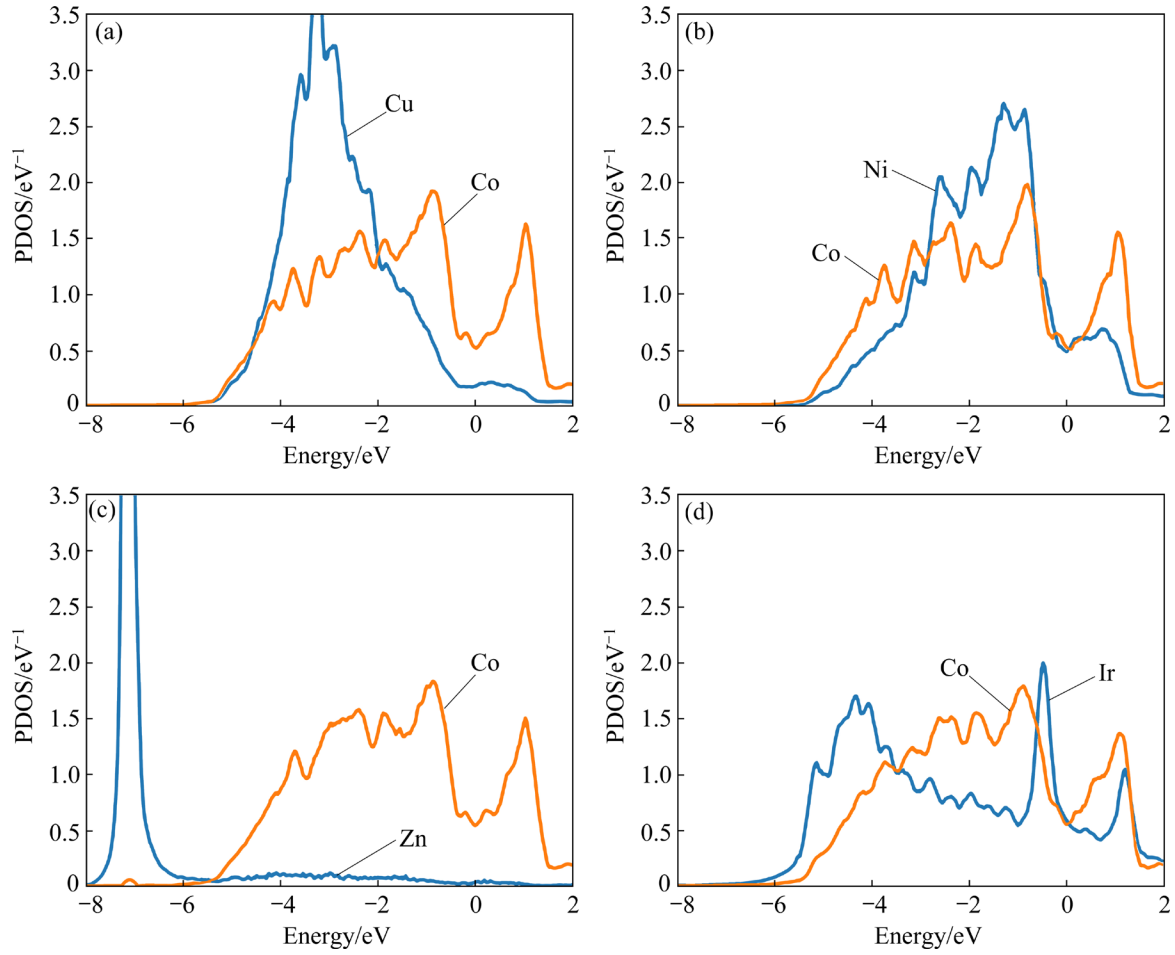

Fig. 8 PDOS of substituted TMs of Cu (a), Ni (b), Zn (c), and Ir (d) and their nearest host Co atoms with respect to substituted atoms

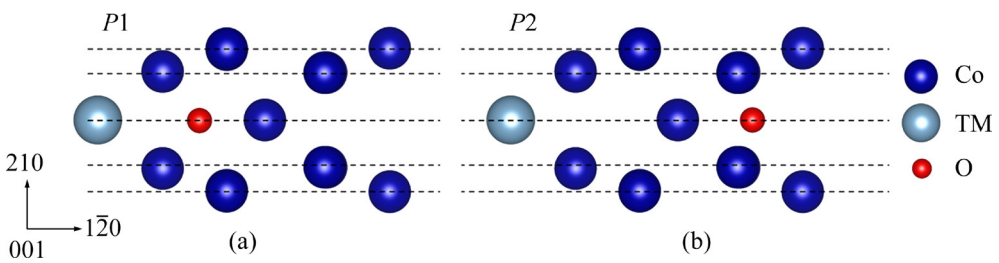

Fig. 9 Two different doping sites for O atoms at GBs, denoted as *P*1 (a) and *P*2 (b), respectively

Nb, Mo, Tc, Ru, Hf, Ta, W, Re, Os, and Ir reduce the E_{seg}^{GB} of O atom, indicating that O atoms are more likely to segregate at the GBs. On the other hand, the existence of Sc, Ni, Cu, Zn, Y, Rh, Pd, Ag, Cd, La, Pt, Au and Hg increases the E_{seg}^{GB} of the O atoms, thereby inhibiting the segregation of O atoms at the GBs. The GB energy with both TM and O is compared with that only with TMs, as shown in Fig. 11. For all 3d TMs, 4d TMs from Y to Ru, and 5d TMs from La to W, the presence of O contributes to the further reduction of GB energy.

The strengthening potency energy η of GB with TM and O atoms is plotted in Fig. 12, where the black dashed line represents the value of GB with only the O atom. When the O atom exists, the η of each system is greatly reduced, of which the degree depends on the type of TM. This indicates that the strength of the GB would be significantly deteriorated by O. But Cr, Hf, Ta, W, Re, Os, Ir, and Pt can alleviate the weakening induced by O.

Figure 13 show the CCD plots of the GB with the Cu−O, Ni−O, Zn−O, and Ir−O aggregations, respectively. We found that the O atom obtains many transferred electrons from the neighboring TM and Co atoms, thereby weakening the bonding strength between TM and Co atoms. In the case of the Ir−O aggregation, a higher charge density, compared with the other TM−O aggregations, is maintained between the TM and Co atoms, which weakens the influence of O on the GB strength. Combined with the strengthening effect of TM on the GBs in the presence of O, we can infer that the Co−TM interaction plays a dominant role in the GB strength.

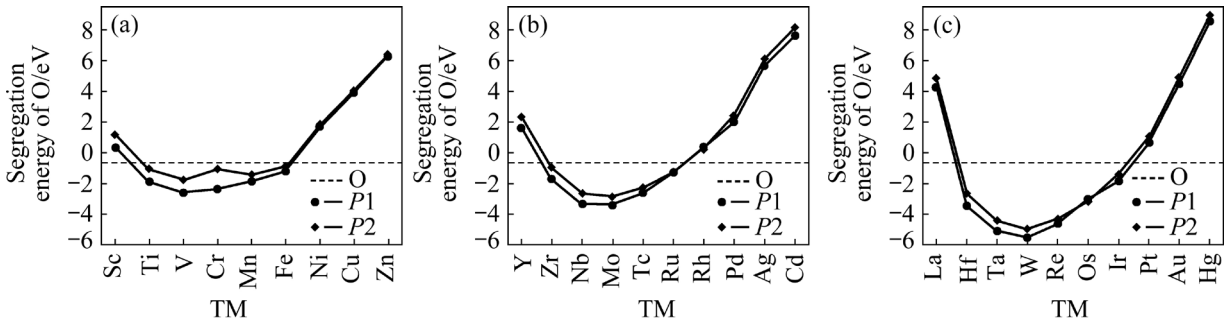

Fig. 10 Segregation energy of O at GBs in the presence of 3d (a), 4d (b) and 5d (c) TMs

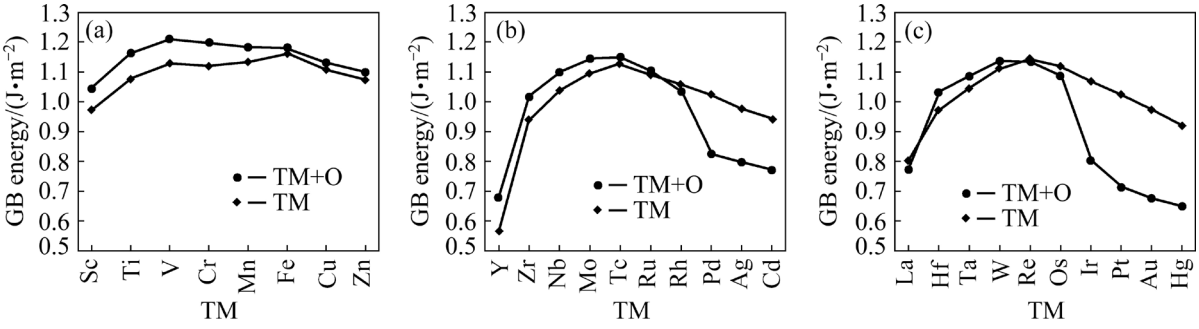

Fig. 11 Energy of GBs with or without O atoms and 3d (a), 4d (b) and 5d (c) TMs

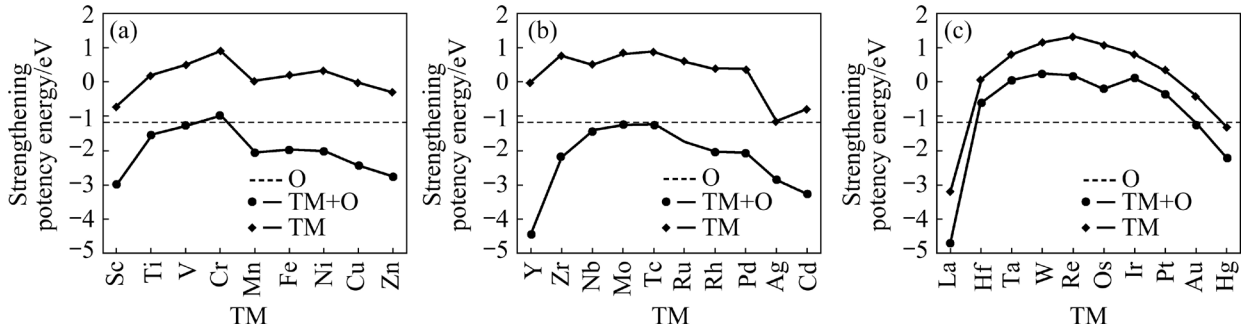

Fig. 12 Strengthening potency energy of GBs with or without O atoms and 3d (a), 4d (b) and 5d (c) TMs

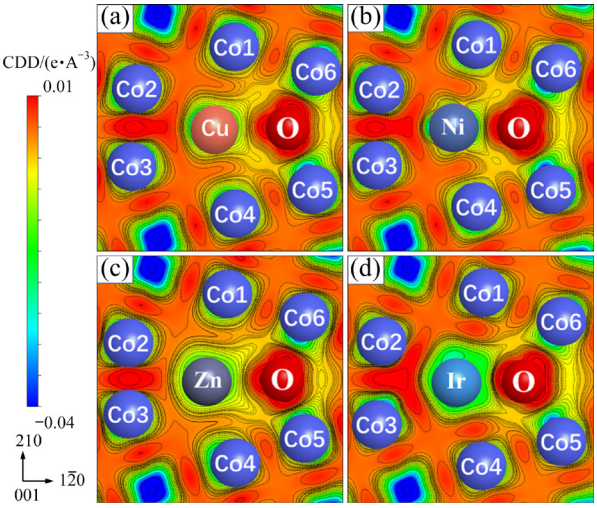

Fig. 13 CDD plots of (001) plane of GBs with Cu−O (a), Ni−O (b), Zn−O (c) and Ir−O (d)

Figure 14 shows the PDOS of the GBs with the Cu−O, Ni−O, Zn−O, and Ir−O aggregations. By comparing with Fig. 8, the weakening effect of the O atom on the GB may be caused by the interactions between the s-orbit of the TMs (including the host Co atoms) and the p-orbit of O, which weakens the bonding strength between the TM and Co atoms. In particular, the d-state of Zn overlaps considerably with the p-state of O, indicating that there is a strong interaction between the O and Zn atoms, which further weakens the GB strength by weakening the TM−Co interaction.

4 Conclusions

(1) The segregation energy profile shows that all TMs tend to segregate towards $\Sigma5(210)[001]$ GB by reducing the GB energy. The magnitude of the reduction of GB energy is closely related to the atomic radius, that is, TM with a larger radius can reduce the GB energy more effectively.

(2) The segregation of TMs has a significant effect on the strength of GB, and this strengthening or weakening effect is determined by the interaction between TM and the nearby Co atoms. The charge density difference near the GB reveals a strong correlation between the strengthening or weakening effect and charge distribution. The analysis of the partial density of states shows that the strengthening effect originates from the strong d-electron hybridization between the TM and Co atoms.

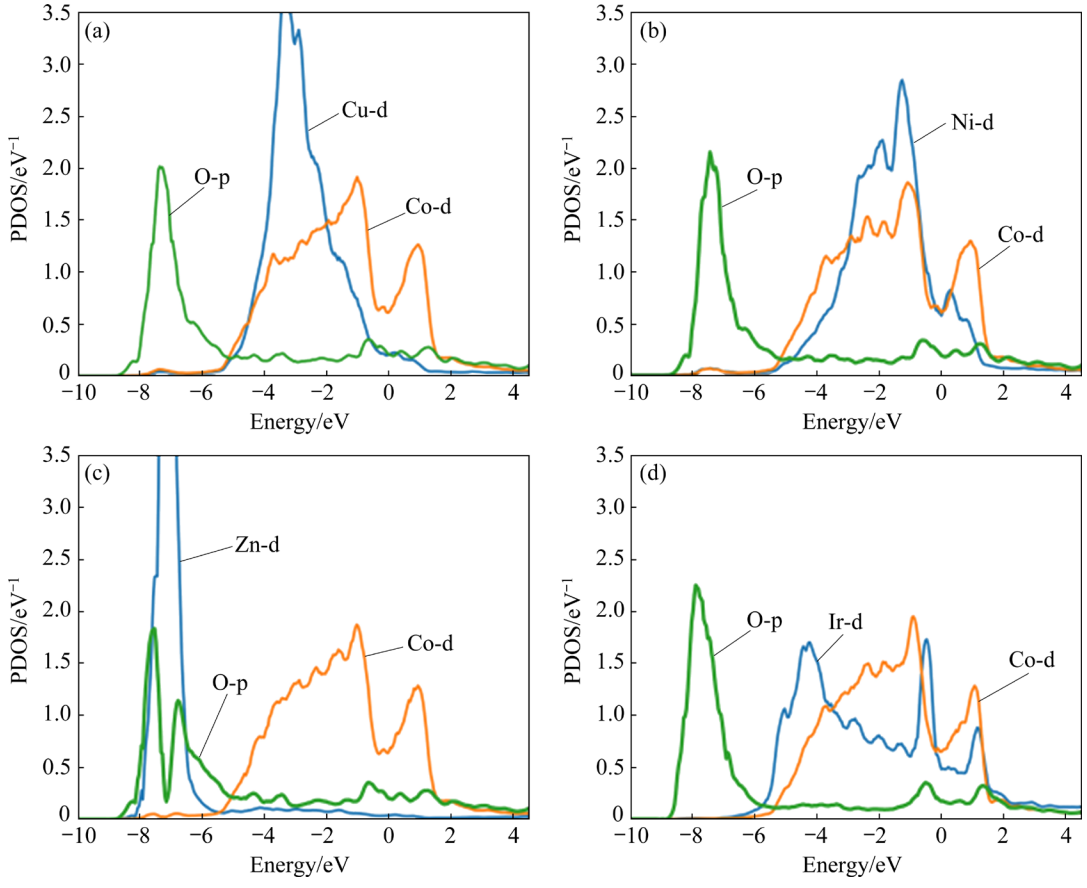

Fig. 14 PDOS of substituted Cu (a), Ni (b), Zn (c), and Ir (d), as well as their nearest host Co and O atoms

(3) The appearance of O atoms will weaken the GBs. This weakening effect caused by O is mainly attributed to the interactions between the p-orbits of O and the s-orbit of the surrounding TM and Co atoms, which weakens the bond between TM and Co. It is found that the segregation of Cr, Hf, Ta, W, Re, Os, Ir and Pt can weaken the interaction between TM and O, and then strengthen the interaction between TM and Co atoms to achieve the purpose of weakening the effect of O atoms on the GBs.

(4) The findings of this work reveal the influence of the segregated TM atoms and their coupling with O atoms on the stability and strength of the GBs of Co, which provide important theoretical guidance for the design of high-performance Co-based superalloys.

Acknowledgments

This work was supported by the Key-Area Research and Development Program of Guangdong Province, China (No. 2019B010943001), and the National Natural Science Foundation of China (No. 51831007).

References

[1] GAO S, SONG Z F, HE B, ZHOU L Z, HOU J S. Effect of Ta addition on solidification microstructure and element segregation of IN617B nickel-base superalloy [J]. Transactions of Nonferrous Metals Society of China, 2022, 32: 559–568.

[2] SATO J, OMORI T, OIKAWA K, OHNUMA I, KAINUMA R, ISHIDA K. Cobalt-base high-temperature alloys [J]. Science, 2006, 312: 90−91.

[3] SUZUKI A, INUI H, POLLOCK T M. $L1_2$-strengthened cobalt-base superalloys [J]. Annual Review of Materials Research, 2015, 45: 345−368.

[4] POLLOCK T M, DIBBERN J, TSUNEKANE M, ZHU J, SUZUKI A. New Co-based γ−γ' high-temperature alloys [J]. JOM, 2010, 62: 58−63.

[5] BAUER A, NEUMEIER S, PYCZAK F, GÖKEN M. Microstructure and creep strength of different γ/γ'-strengthened Co-base superalloy variants [J]. Scripta Materialia, 2010, 63: 1197−1200.

[6] SUZUKI A, POLLOCK T M. High-temperature strength and deformation of γ/γ' two-phase Co−Al−W-base alloys [J]. Acta Materialia, 2008, 56: 1288−1297.

[7] FREUND L P, MESSÉ O M D M, BARNARD J S, GÖKEN M, NEUMEIER S, RAE C M F. Segregation assisted microtwinning during creep of a polycrystalline $L1_2$-hardened Co-base superalloy [J]. Acta Materialia, 2017, 123: 295−304.

[8] QUAN Guo-zheng, ZHANG Yu-qing, ZHANG Pu, MA Yao-yao, WANG Wei-yong. Correspondence between low-energy twin boundary density and thermal-plastic deformation parameters in nickel-based superalloy [J]. Transactions of Nonferrous Metals Society of China, 2021, 31: 438−455.

[9] CHENG Bo, WU Dong-jiang, ZHANG Chao, CHAI Dong-sheng, MA Guang-yi. Transformation mechanism of secondary phase and its effect on intergranular corrosion in laser wire filling welding Ni-based alloy/304 stainless steel [J]. Transactions of Nonferrous Metals Society of China, 2021, 31: 715−725.

[10] BOCCHINI P J, SUDBRACK C K, NOEBE R D, DUNAND D C, SEIDMAN D N. Microstructural and creep properties of boron- and zirconium-containing cobalt-based superalloys [J]. Materials Science and Engineering A, 2017, 682: 260−269.

[11] HOOSHMAND M S, NIU C, TRINKLE D R, GHAZISAEIDI M. First-principles prediction of oxygen diffusivity near the $(10\bar{1}2)$ twin boundary in titanium [J]. Acta Materialia, 2018, 156: 11−19.

[12] KLEIN L, KILLIAN M S, VIRTANEN S. The effect of nickel and silicon addition on some oxidation properties of novel Co-based high temperature alloys [J]. Corrosion Science, 2013, 69: 43−49.

[13] HAJILOU T, TAJI I, CHRISTIEN F, HE S, SCHEIBER D, ECKER W, PIPPAN R, RAZUMOVSKIY V I, BARNOUSH A. Hydrogen-enhanced intergranular failure of sulfur-doped nickel grain boundary: In situ electrochemical micro-cantilever bending vs. DFT [J]. Materials Science and Engineering A, 2020, 794: 139967.

[14] RAZUMOVSKIY V I, LOZOVOI A Y, RAZUMOVSKII I M. First-principles-aided design of a new Ni-base superalloy: Influence of transition metal alloying elements on grain boundary and bulk cohesion [J]. Acta Materialia, 2015, 82: 369−377.

[15] VŠIANSKÁ M, VÉMOLOVÁ H, ŠOB M. Segregation of sp-impurities at grain boundaries and surfaces: Comparison of fcc cobalt and nickel [J]. Modelling and Simulation in Materials Science and Engineering, 2017, 25: 085004.

[16] WANG Shen, XIONG Jun, ZENG Qiang, XIONG Min, CHAI Xiao-song, LI Da. Effect of Nb on He segregation behavior in Ni Σ5 grain boundary: First-principles study [J]. Fusion Engineering and Design, 2020, 154: 111549.

[17] ZHAO D D, LØVVIK O M, MARTHINSEN K, LI Y J. Segregation of Mg, Cu and their effects on the strength of Al Σ5(210)[001] symmetrical tilt grain boundary [J]. Acta Materialia, 2018, 145: 235−246.

[18] RAZUMOVSKIY V I, DIVINSKI S V, ROMANER L. Solute segregation in Cu:DFT vs. experiment [J]. Acta Materialia, 2018, 147: 122−132.

[19] RICE J R, WANG J S. Embrittlement of interfaces by solute segregation [J]. Materials Science and Engineering A, 1989, 107: 23−40.

[20] HUANG Zhi-feng, CHEN Fei, SHEN Qiang, ZHANG Lian-meng, RUPERT T J. Combined effects of nonmetallic impurities and planned metallic dopants on grain boundary energy and strength [J]. Acta Materialia, 2019, 166:

113−125.
[21] LOZOVOI A Y, PAXTON A T, FINNIS M W. Structural and chemical embrittlement of grain boundaries by impurities: A general theory and first-principles calculations for copper [J]. Physical Review B, 2006, 74: 1−13.
[22] KRESSE G, JOUBERT D. From ultrasoft pseudopotentials to the projector augmented-wave method [J]. Physical Review B, 1999, 59: 1758−1775.
[23] KRESSE G, FURTHMÜLLER J. Efficiency of ab-initio total energy calculations for metals and semiconductors using a plane-wave basis set [J]. Computational Materials Science, 1996, 6: 15−50.
[24] ROPO M, KOKKO K, VITOS L. Assessing the Perdew−Burke−Ernzerhof exchange-correlation density functional revised for metallic bulk and surface systems [J]. Physical Review B, 2008, 77: 195445.
[25] MONKHORST H J, PACK J D. Special points for Brillouin-zone integrations [J]. Physical Review B, 1976, 13: 5188−5192.
[26] METHFESSEL M, PAXTON A T. High-precision sampling for Brillouin-zone integration in metals [J]. Physical Review B, 1989, 40: 3616−3621.
[27] MA Jian-qiang, ZHONG Fei, LI Shu-suo, SHA Jiang-bo. Microstructure and grain boundary morphology evolution of a novel Co−9Al−9W−2Ta−0.02B alloy doped with yttrium [J]. Rare Metals, 2017, 36: 951−961.

过渡金属元素与氧对钴晶界能与晶界强度作用的第一性原理研究

陈有恒[1]，王翠萍[1,2]，黄 翔[1]，杨 琛[1]，韩佳甲[1,2]，刘兴军[1,3]

1. 厦门大学 材料学院 福建省材料基因工程重点实验室，厦门 361005；
2. 厦门大学 厦门市高性能金属材料重点实验室，厦门 361005；
3. 哈尔滨工业大学 材料基因与大数据研究院，深圳 518055

摘 要：以 Co 的$\Sigma5$(210)[001]晶界为模型，基于第一性原理研究过渡金属元素与氧对钴晶界能与晶界强度的影响。定量分析过渡金属在晶界处的偏析，揭示晶界能与原子半径之间的负相关关系。结果表明，溶质和晶界处基体原子之间的相互作用影响晶界强度。其中，Re、W、Os、Cr、Tc、Mo、Ir、Ta、Zr、Ru、Nb、V、Rh、Pt、Pd 和 Ni 能显著强化晶界，而其他过渡金属会弱化晶界。特别地，Cr、Hf、Ta、W、Re、Os、Ir 和 Pt 能有效缓解 O 原子引起的晶界弱化。

关键词：过滤金属元素；氧；钴基高温合金；第一性原理计算；偏析；晶界能；晶界强度

(Edited by Wei-ping CHEN)